



Radial asymmetries in population receptive field size and cortical magnification factor in early visual cortex

Maria Fatima Silva^a, Jan W. Brascamp^{b,c}, Sónia Ferreira^a, Miguel Castelo-Branco^{a,d},
Seure O. Dumoulin^b, Ben M. Harvey^{b,e,*}

^a Visual Neuroscience Laboratory, Institute for Biomedical Imaging and Life Sciences (IBILI), Faculty of Medicine, University of Coimbra, Azinhaga de Santa Comba, 3000-548 Coimbra, Portugal

^b Experimental Psychology, Helmholtz Institute, Utrecht University, Heidelberglaan 1, 3584 CS Utrecht, The Netherlands

^c Department of Psychology, Michigan State University, East Lansing, MI 48823, USA

^d Institute of Nuclear Sciences Applied to Health (ICNAS), University of Coimbra, Azinhaga de Santa Comba, 3000-548 Coimbra, Portugal

^e Faculty of Psychology and Education Sciences, University of Coimbra, Rua do Colégio Novo, 3001-802 Coimbra, Portugal

ARTICLE INFO

Keywords:

Visual cortex
Polar angle
Asymmetry
Population receptive field (pRF)
Cortical magnification factor (CMF)

ABSTRACT

Human visual cortex does not represent the whole visual field with the same detail. Changes in receptive field size, population receptive field (pRF) size and cortical magnification factor (CMF) with eccentricity are well established, and associated with changes in visual acuity with eccentricity. Visual acuity also changes across polar angle. However, it remains unclear how RF size, pRF size and CMF change across polar angle. Here, we examine differences in pRF size and CMF across polar angle in V1, V2 and V3 using pRF modeling of human fMRI data. In these visual field maps, we find smaller pRFs and larger CMFs in horizontal (left and right) than vertical (upper and lower) visual field quadrants. Differences increase with eccentricity, approximately in proportion to average pRF size and CMF. Similarly, we find larger CMFs in the lower than upper quadrant, and again differences increase with eccentricity. However, pRF size differences between lower and upper quadrants change direction with eccentricity. Finally, we find slightly smaller pRFs in the left than right quadrants of V2 and V3, though this difference is very small, and we find no differences in V1 and no differences in CMF. Moreover, differences in pRF size and CMF vary gradually with polar angle and are not limited to the meridians or visual field map discontinuities. pRF size and CMF differences do not consistently follow patterns of cortical curvature, despite the link between cortical curvature and polar angle in V1. Thus, the early human visual cortex has a radially asymmetric representation of the visual field. These asymmetries may underlie consistent reports of asymmetries in perceptual abilities.

Introduction

The representation of visual space in the cortical visual field maps influences how we see the world. As visual field eccentricity increases across a visual field map, neural receptive field (RF) and population receptive field (pRF) sizes increase, and cortical magnification factor (CMF) decreases (Dow et al., 1981; Duncan and Boynton, 2003; Harvey and Dumoulin, 2011; Hubel and Wiesel, 1974; Smith et al., 2001). Both increases in RF/pRF size and decreases in CMF imply a coarser neural representation of visual space. Indeed, visual acuity and other metrics of perceptual performance decrease with visual field eccentricity (Duncan and Boynton, 2003; Strasburger et al., 2011). Recent human fMRI studies have linked differences in perceptual performance to the large

differences in pRF size and CMF across eccentricity (Duncan and Boynton, 2003) and between individuals (Song et al., 2015).

There is also behavioral evidence of smaller differences in visual perceptual performance for stimuli presented at the same eccentricity at different polar angles: above, below, left and right of fixation (for a review see (Karim and Kojima, 2010)). However, it remains unclear how RF/pRF size and CMF change with polar angle. Given these perceptual asymmetries, we hypothesize that there may be small variations in RF size and CMF across polar angle in early visual cortex. Here we set out to measure these variations using pRF modeling from fMRI data.

Several technical limitations have complicated neurophysiological investigation of this question. First, large differences in receptive field size and CMF across eccentricity can obscure smaller differences across

* Corresponding Author. Department of Experimental Psychology, Helmholtz Institute, Utrecht University, Heidelberglaan 1, 3584 CS Utrecht, The Netherlands.
E-mail address: b.m.harvey@uu.nl (B.M. Harvey).

polar angle. Differences across polar angle are difficult to resolve if comparing recordings made at different eccentricities, and it is very difficult to find pairs of individual neurons at the same eccentricity in single-unit recordings. Second, individual animals and humans differ considerably in RF size, pRF size and CMF (Dougherty et al., 2003; Harvey and Dumoulin, 2011; Van Essen et al., 1984), necessitating large numbers of measurements in the same individual. It is difficult to measure from large numbers of single neurons in a single visual field map of a single animal. fMRI measurements are well suited to analyze these changes across the visual field map because they distribute recording sites densely and evenly across cortex. Taking advantage of this technique, we can make paired comparisons between recording sites at different polar angles, but at the same eccentricity and in the same subject. Third, changes in CMF with polar angle differ between species and individual animals (Van Essen et al., 1984), so it is unclear how results from small numbers of primates would generalize to the human population. Here we used a larger number of human subjects.

Despite these complications, some neurophysiological studies have shown changes in CMF with polar angle in V1 (Adams and Horton, 2003; Tootell et al., 1988; Van Essen et al., 1984). However, these CMF differences may simply result from V1's strong relationships between polar angle and cortical folding, which could cause certain polar angles to cover larger areas of the surface (i.e. have larger CMF) (Dahlem and Tusch, 2012). Therefore, CMF differences may be a byproduct of anatomical constraints and have no functional consequence. On the other hand, these CMF differences may have functional consequences regardless of whether they result from cortical folding differences. These possibilities could be distinguished by examining changes in pRF size together with CMF: RF/pRF size and CMF differences between individuals and across eccentricity are closely related (Harvey and Dumoulin, 2011; Hubel and Wiesel, 1974). Furthermore, V1's relationships between cortical folding, available cortical surface area and polar angle would not apply to V2 and V3. However, functional properties of one visual field map are often mirrored in its neighbors. Therefore, we examine changes in pRF size as well as CMF across both polar angle and cortical curvature, and extend these measurements into V2 and V3.

With this approach, we revealed smaller pRFs and larger CMFs in the horizontal (left and right) than the vertical (upper and lower) visual field quadrants, implying a finer representation of the visual field in these quadrants. pRFs were also smaller and CMFs larger in the lower than upper quadrant in most visual field maps, and pRFs were smaller in the left than right quadrant in V2 and V3. These differences typically increased with eccentricity. They were not limited to the meridians or discontinuities in the visual field maps, but varied gradually with polar angle to reach maxima and minima at the meridians. These results demonstrate that the early human visual cortex does not have a radially symmetrical representation of the visual field. We speculate that these small asymmetries in the neural representation may underlie reports of asymmetries in perceptual performance in different parts of the visual field.

Materials and methods

The data acquisition and most of the analyses follow the protocols used in a previous study of the relationship between pRF size and CMF and across eccentricity (Harvey and Dumoulin, 2011). Here, we added eleven further subjects to our existing pool of eleven right-handed subjects, and added new analyses to examine changes in pRF size and CMF across polar angle.

Subjects

Twenty-two healthy right-handed subjects participated in this study (age range 22–46 years, 8 female). To restrict comparisons between left and right visual quadrants to subjects with the same dominant hemisphere, we excluded left-handed subjects using the Edinburgh

handedness inventory (Oldfield, 1971). All subjects had normal or corrected-to-normal visual acuity. Experiments were undertaken with the informed written consent of each subject. All experimental procedures were cleared by the ethics committee of University Medical Center Utrecht.

MRI acquisition

We acquired functional and anatomical MRI data on a Philips Achieva 3T scanner (Philips Medical Systems, Best, Netherlands) with a Quasar Dual gradient set. We acquired T1-weighted anatomical MRI data at $0.75 \times 0.75 \times 0.8$ mm spatial resolution. Flip angle was set to 8° , repetition time (TR) was 10.029 ms, and echo time (TE) was 4.6 ms. We acquired T2*-weighted functional 2D echo planar images at $2.5 \times 2.5 \times 2.5$ mm spatial resolution, with 24 slices. Flip angle was set to 70° , TR was 1500 ms, and TE was 30 ms. Each functional scan was 248 time frames (372 s) in duration, the first eight time frames (12 s) of which were discarded. We acquired seven to ten repeated scans within the same session for each subject.

Stimulus presentation setup

We back-projected visual stimuli onto a 101×76 cm screen viewed through a mirror attached to the MRI coil. The screen was 348 cm from the subject's eyes, via the mirror, and its resolution was 800×600 pixels. We constrained stimuli to a circular area filling the screen's vertical dimension. Any area outside this circle remained at constant mean luminance. The stimulus circle was 6.25° of visual angle in radius, from the subject's viewpoint.

Visual stimuli

We generated the visual stimuli using the PsychToolbox for Matlab (Brainard, 1997; Pelli, 1997). They consisted of drifting bar apertures at various orientations, which exposed a checkerboard pattern with 100% contrast moving parallel to the bar's orientation (Dumoulin and Wandell, 2008). Alternating rows of checks moved in opposite directions. The motion direction of the checks reversed at random intervals, with 4 s minimum between reversals. The bar width and the fundamental spatial frequency of the checks was 1.56° . The bar stepped across the stimulus aperture in 20 equally spaced steps of 0.625° each. The bar stepped at the start of each functional volume acquisition, so took 20 TRs (30 s) to cross the stimulus circle. In each scan, we showed 4 bar orientations each stepping in two opposite directions, making a total of 8 bar motion directions (upwards, downwards, left, and right, alternated with four diagonals). We displayed 30 s of mean luminance display with no bar after each horizontal or vertical bar orientation pass, at regularly spaced intervals through the scanning run.

Subjects fixated a dot in the center of the visual stimulus, which changed colors at random intervals between red and green. Subjects pressed a button on a response box every time the color changed to ensure attention and fixation were maintained. Color changes were every 3 s on average, with a minimum change interval of 1.8 s. We discarded any scan where detection performance dropped below 75% (2 scans of 1 subject).

Preprocessing of anatomical and functional images

We analyzed fMRI data in the mrVista software package for MATLAB, available at (<http://white.stanford.edu/software/>). For each subject, we resampled T1-weighted anatomical scans to 1 mm^3 resolution. We automatically segmented the resulting anatomical image using FSL (Smith et al., 2004), then hand-edited it to minimize segmentation errors (Teo et al., 1997). We reconstructed the cortical surface at the gray-white matter border. We rendered this as a smoothed 3D surface (Wandell et al., 2000). We measured and corrected for head movement and motion

artifacts between and within functional scans (Nestares and Heeger, 2000). We then averaged functional data across scans, aligned this to anatomical scans (Nestares and Heeger, 2000) and interpolated it to the anatomical segmentation.

fMRI data-analysis

We estimated pRF positions and sizes from the fMRI data and the time course of presented visual stimulus positions (Dumoulin and Wandell, 2008). The BOLD response of each recording site (voxel) was predicted using a two-dimensional circular Gaussian pRF model. This modeled the location (x and y parameters) and size (σ) of the pRF: the area where the recording site responds most strongly to the stimulus. Convolution of the modeled pRF, the stimulus sequence and a canonical BOLD hemodynamic response function (HRF) (Friston et al., 1998; Glover, 1999; Worsley et al., 2002) gave a candidate predicted fMRI time course for each combination of x , y and σ parameters. The pRF parameters for each recording site were determined by finding the pRF parameters with the smallest sum of squared errors between the predicted and observed fMRI time series.

After estimating the pRF parameters for each subject, the HRF parameters were determined by minimizing the RSS between the predicted and observed BOLD responses over the entire recorded cortex to give the final model fit (Harvey and Dumoulin, 2011).

The polar angle and eccentricity maps of the pRF centers of each recording site were rendered onto an inflated cortical surface (Wandell et al., 2000), and the positions of V1, V2 and V3 were determined and defined as regions of interest (ROIs) by relation to visual field representation (Serenio et al., 1995; Wandell et al., 2007). Areas of low mean fMRI signal, corresponding to pial draining veins (Olman et al., 2007; Winawer et al., 2010) were excluded from subsequent analysis.

We determined the CMF for every recording site on the gray-white matter border independently. All analysis of pRF and CMF was therefore restricted to recording sites on the gray-white matter border. Gray matter thickness was ignored, effectively treating the gray-white matter border as the cortical surface. At each recording site we computed the distance (mm) to neighboring locations (vertices) along the cortical surface mesh. Neighboring recording sites with poor pRF model fits (variance explained < 30%) were removed from this computation, as were recording sites outside the ROI. In approximately 70% of recording sites, this yielded six to eight valid neighbors, but approximately 1% of recording sites had a single valid neighbor and 1% had eleven or twelve. Recording sites with no neighbors were excluded from further analysis. To compute the CMF this cortical distance was divided by the change in preferred pRF location (degrees of visual angle) of the same recording sites.

Determining pRF size and CMF within each visual field quadrant

In the following description and in the results section, we describe visual field quadrants in terms of visual space representations rather than their cortical representations: the left visual space quadrant is in the right hemisphere, the lower visual space quadrant of V1 is on the upper bank of the calcarine sulcus, and so on.

For each subject, we first defined visual field map quadrants above (upper quadrant), below (lower quadrant), left and right of fixation, using the location of each recording site's pRF preferred position. We excluded any recording sites whose pRF models explain less than 30% of the fMRI signal variance (11% of recording sites, Supplementary Fig. 1) or whose pRF centers lay in the ipsilateral hemifield. We also excluded recording sites with pRF eccentricities below 0.5° , as this part of the visual field representation is difficult to accurately map. Finally, we excluded recording sites with pRF eccentricities above 5.5° , as much of the pRFs of these sites falls outside the stimulus area. There were on average 56 recording sites per quadrant in V1, 51 in V2 and 44 in V3.

Binning pRF sizes and CMFs

We grouped recording sites from each quadrant in each subject into eccentricity bins before grouping data across subjects and comparing between quadrants. This allows us to compare bins from the same eccentricity and subject in paired statistical tests. This binning and pairing disregards the large differences in CMF and pRF size across eccentricity and between subjects.

For each visual field map quadrant in each subject, we divided the recording sites into bins by their pRF eccentricity, each covering an eccentricity range of 0.25° . This yielded a maximum of 21 bins per quadrant (i.e. $0.375\text{--}0.625^\circ$, $0.625\text{--}0.875^\circ$, ..., $5.375\text{--}5.625^\circ$), though not all of these bins contained data for comparison in each subject or each quadrant. Each bin groups the properties of multiple independent fMRI recording sites, thus down-sampling the acquired data. For each bin, we determined the mean pRF size and inverse CMF. Inverse CMF ($^\circ/\text{mm}$) is approximately proportional to eccentricity and pRF size, making it easier to examine correlations between inverse CMF and eccentricity. Together with left, right, upper and lower quadrants, we also compare the combined vertical quadrants (i.e. both the upper and lower quadrants) to the combined horizontal quadrants (i.e. both the left and right quadrants). These are the means of bins in left and right quadrants, and upper and lower quadrants respectively. This comparison is analogous to comparisons between the horizontal and vertical meridians that are common in primate neurophysiological studies (Adams and Horton, 2003; Tootell et al., 1988; Van Essen et al., 1984) and human perceptual studies (Carrasco et al., 1995, 2001; Rijdsdijk et al., 1980; Rovamo and Virsu, 1979). To compare bins across quadrants, we then determine the difference between bin means at the same eccentricity in the same subject. Bins pairs were excluded from comparison if both bins did not contain at least one recording site.

Grouping across subjects and comparing between quadrants

We then put the differences between bins from opposite quadrants from all subjects into a group. We used two-tailed paired t -tests to determine whether the group of differences for all subjects and eccentricities was significantly different from zero. We used two-tailed Wilcoxon signed rank tests, a non-parametric alternative to a paired t -test, to confirm that these yielded the same pattern of significant differences, and found similar results.

To test whether differences between quadrants change with eccentricity, we first took the difference between eccentricity bins from opposite quadrants, again grouped across subjects. We used Spearman's (non-parametric) correlation to test for relationships between the difference of bin means and each bin's visual field eccentricity. This yields the correlations described in the results.

As pRF size and CMF change systematically with eccentricity, we also examine differences between paired bins from opposite quadrants expressed as a ratio of pRF size or inverse CMF. We took each difference between paired bins and divided this by the pair's average pRF size or inverse CMF, giving the difference in pRF size or CMF as a ratio of pRF size or CMF. As above, we used two-tailed paired t -tests to determine whether the group of differences for all subjects and eccentricities was significantly different from zero, and used Spearman's (non-parametric) correlation to test for relationships between the difference of bin means and each bin's visual field eccentricity.

For visualization in Figs. 1–3 Panels A & B, we also took the group of recording sites across all subjects, and divided these into quadrants. For each quadrant, we then divided the recording sites into bins by their pRF eccentricity, each 0.25° wide. In other words, for visualization we grouped recording sites across subjects before binning by eccentricity, while elsewhere we binned recording sites by eccentricity before grouping across subjects. For each bin, we determined the mean pRF size and CMF and the standard errors of these means. We repeated are comparisons using differences between the all-subject bin means, giving

similar results.

Fits of pRF size and CMF versus eccentricity

The pRF size versus eccentricity relationship was described by the following equation:

$$\sigma_{pRF} = ax + b \quad (1)$$

where σ_{pRF} is pRF size, x is eccentricity, a and b are the slope and intercept respectively. The a and b terms were estimated by minimizing the sum of squared errors (RSS) to the eccentricity-binned data, with each error weighted by the inverse of the standard error of the mean in that bin. In a similar fashion, the CMF versus eccentricity function was described by the following equation, also used in other studies (Dougherty et al., 2003; Engel et al., 1994; Schira et al., 2010; Sereno et al., 1995):

$$CMF = \frac{1}{cx + d} \quad (2)$$

where CMF is cortical magnification factor, x is eccentricity, and c and d are the slope and intercept respectively.

Compensating for effects of eccentricity and plotting changes across polar angle

Next, we plotted pRF size and CMF changes across polar angle (Fig. 4). These changes are obscured by larger changes in pRF size and CMF with eccentricity and between subjects, so we first compensated for these effects by linear regression.

For each subject, we first took the pRF sizes, CMFs and eccentricities of each recording site. We fit the linear relationship between pRF size and eccentricity (Equation (1)) and the inverse linear relationship between CMF and eccentricity (Equation (2)). For each recording site, we then evaluated these relationships at the recording site's eccentricity, and subtract these values from the pRF size and CMF of the recording site. This yields pRF sizes and CMFs that are corrected for these relationships to eccentricity. This procedure also compensates for the large differences in pRF size and CMF between subjects (Dougherty et al., 2003; Harvey and Dumoulin, 2011).

We then took the eccentricity-corrected pRF sizes and CMFs of recording sites from all subjects and grouped these into 32 evenly-spaced polar angle bins. For each bin, we took the median pRF size and CMF. We determined confidence intervals on these medians by taking the median pRF size or CMF from the recording sites in 1000 bootstrapped selections of subjects, without replacement. We determined 95% confidence intervals by taking the 2.5th and 97.5th percentiles of these bootstrapped sample medians.

Plotting changes across cortical curvature

We also used this same group of eccentricity-corrected pRF sizes and CMFs to examine the effects of cortical curvature on these properties, again compensating for the large changes in these properties with eccentricity and between subject. We determined the cortical curvature at the same recording sites from a rendered mesh of the cortical surface. We used the cortical curvature values to group all recording sites into a 41 evenly-spaced bins of cortical curvature ranging from -0.5 to 0.5 . Many of the bins at the extremes of this range contained no recording sites. We took the median of the eccentricity-corrected pRF sizes and CMFs of the recording sites within each bin and used a Spearman's correlation to examine the relationship between these properties and cortical curvature. Again, we determined confidence intervals on these medians by taking the median pRF size or CMF from the recording sites in 1000 bootstrapped selections of subjects, without replacement.

Results

pRF sizes are smaller and CMF is larger in the horizontal than the vertical quadrants

The largest difference we find is between horizontal quadrants (i.e. left and right quadrants combined) and vertical quadrants (i.e. upper and lower quadrants combined). This comparison follows comparisons made in both primate neurophysiology (Adams and Horton, 2003; Tootell et al., 1988; Van Essen et al., 1984) and human perceptual studies (Carrasco et al., 1995, 2001; Rijdsdijk et al., 1980; Rovamo and Virsu, 1979). In all quadrants, pRF size increases and CMF decreases with eccentricity (Fig. 1A, B). However, at all eccentricities there are differences between quadrants. The vertical quadrants of V1, V2 and V3 have larger pRF sizes than the horizontal quadrants (Fig. 1C). In line with these differences in pRF size (Harvey and Dumoulin, 2011), the vertical quadrants of V1, V2 and V3 have smaller CMFs than the horizontal quadrants (Fig. 1D). Similar results are found if recording sites in the same eccentricity range are averaged across all subjects before comparison (Supplementary Fig. 2). Data from representative individual subjects is shown in Supplementary Fig. 3. Both of these differences in pRF size and CMF suggest a finer neural representation of the horizontal than the vertical visual quadrants.

These differences in pRF size and CMF often increase with eccentricity (Fig. 1). In V1 and V3, vertical quadrant pRF sizes increase more strongly with eccentricity than horizontal quadrant pRF sizes (Fig. 1C), though there is no significant correlation in V2. The mean pRF size at the same eccentricity grouped across all subjects is similarly significantly correlated with eccentricity in all visual field maps (Supplementary Fig. 2A). Similarly, vertical quadrant CMFs decrease more strongly with eccentricity than horizontal quadrant CMFs in V1 and V3, though there is no significant correlation in V2 (Fig. 1D). The mean CMF at the same eccentricity grouped across all subjects is similarly significantly correlated with eccentricity in V2 only (Supplementary Fig. 2B). Therefore, the relative overrepresentation of the horizontal quadrants increases with eccentricity.

As pRF sizes and inverse CMFs typically increase with eccentricity, we ask how these comparisons are affected by expressing pRF size differences as the ratio of pRF size, and CMF differences as a ratio of inverse CMF. We again find that vertical quadrants have larger pRF sizes than the horizontal quadrants (V1: $t = 9.5$, $p = 1 \times 10^{-18}$, $n = 261$. V2: $t = 3.8$, $p = 0.0002$, $n = 267$. V3: $t = 15.3$, $p = 2 \times 10^{-37}$, $n = 245$), but cease to find significant correlations between pRF size difference and eccentricity. Across all eccentricities, the pRF size difference between horizontal and vertical quadrants remains about 9.2% of V1's pRF size, 10.3% of V2's pRF size and 16.4% of V3's pRF size. Similarly, vertical quadrants have smaller CMFs than the horizontal quadrants (V1: $t = 6.3$, $p = 2 \times 10^{-9}$, $n = 193$. V2: $t = 8.1$, $p = 5 \times 10^{-14}$, $n = 193$. V3: $t = 3.8$, $p = 0.0002$, $n = 195$), but CMF differences are no longer significantly correlated with eccentricity. Across all eccentricities, the CMF difference between horizontal and vertical quadrants remains about 6.7% of V1's inverse CMF, 18.5% of V2's inverse CMF and 5.7% of V3's inverse CMF.

CMF is larger in the lower quadrants in V1, V2 and V3. pRF size differences change with eccentricity

When considering all eccentricities together, we find less clear and consistent pRF size differences between upper and lower visual field quadrants. The lower quadrant of V1 has smaller pRF sizes than the upper quadrant, but there are no significant differences in V2 or V3 (Fig. 2). In line with V1's differences in pRF size, the lower quadrants of V1, V2 and V3 have larger CMFs than the upper quadrants. Similar results are found if differences at the same eccentricities are averaged across subjects before comparison (Supplementary Fig. 4). Data from individual subjects is shown in Supplementary Fig. 5. All CMF differences, together with the pRF size difference in V1, suggest a finer neural representation of the

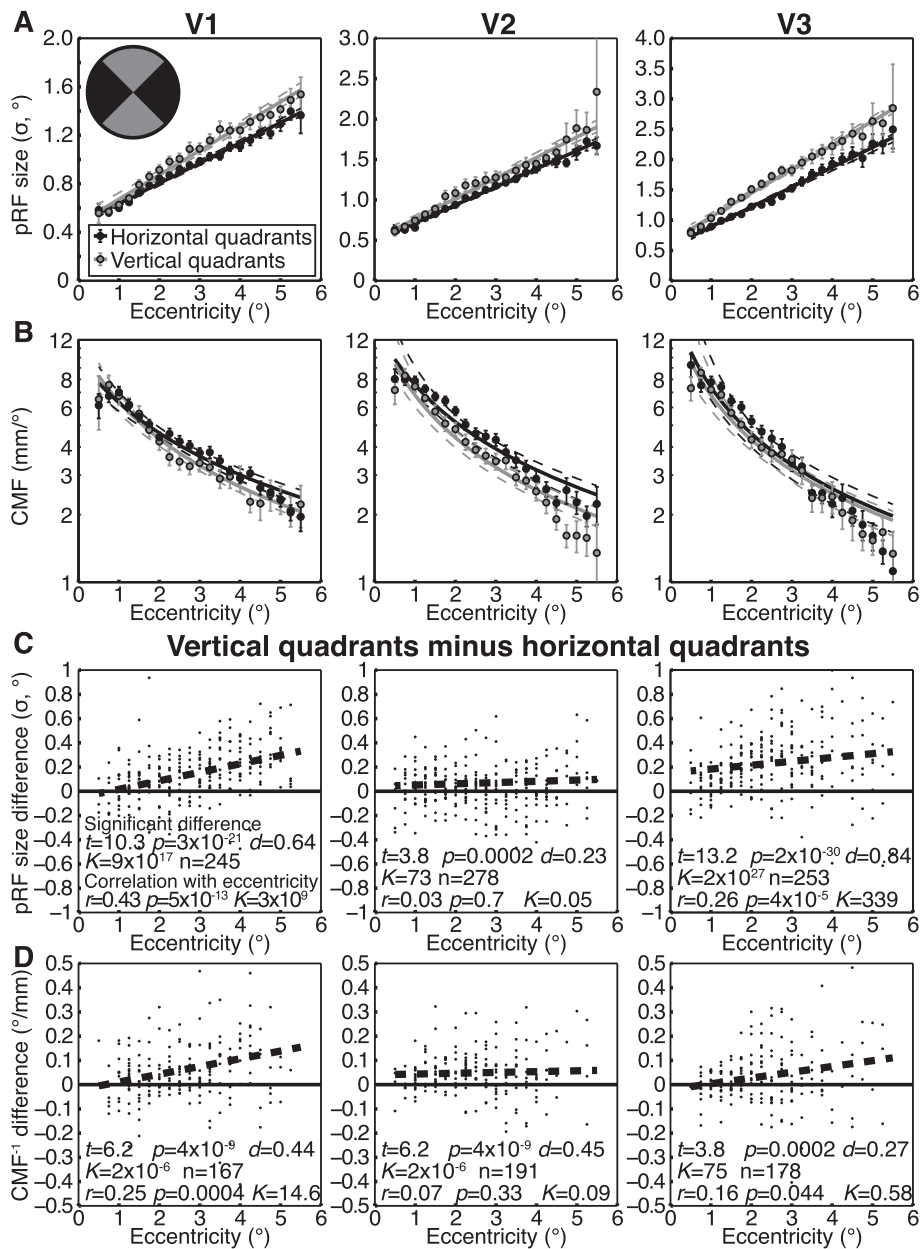


Fig. 1. Comparisons of pRF size and CMF between groups of recording sites (voxels) in quadrants centered around the vertical and horizontal visual field meridians, paired for eccentricity and subject identity. (A) In data grouped across all subjects, pRF sizes increase with eccentricity and pRF sizes are smaller in the horizontal than the vertical quadrants. (B) Similarly, CMF decreases with eccentricity and CMFs are larger in the horizontal quadrants. (C) Differences between paired bins from individual subjects show pRF sizes are significantly larger in the vertical than the horizontal quadrants in V1, V2 and V3. This difference increases significantly with eccentricity in V1 and V3, but not V2. (D) Conversely, CMFs are significantly larger in horizontal than the vertical quadrants in V1, V2 and V3. This difference increases significantly with eccentricity in V1 and V3, but not V2. Note that this plot shows inverse CMF: this is linearly related to eccentricity, but reverses the sign of the difference. The t values and their associated p values are results of paired samples t -tests between the means of bins of recording sites in different quadrants at the same eccentricities in the same subjects. r values and their associated p values are results of Spearman's correlations of the difference between quadrants with eccentricity. K is the Bayes factor for these paired t -tests and Spearman's correlations. d is Cohen's d , the effect size of the paired t -tests.

lower than the upper visual quadrant.

These mixed differences in pRF size become more consistent when considering changes across eccentricity (Fig. 2C). Differences in pRF size are correlated with eccentricity: upper quadrant pRF sizes increase more strongly with eccentricity than lower quadrant pRF sizes in V1, V2 and V3. So while the lower quadrant tends to have larger pRFs than the upper quadrant in the central visual field representation (for example, less than 2° eccentricity: V1, $p = 0.14$; V2, $p = 0.001$; V3, $p = 0.0009$), it tends to have smaller pRFs in the peripheral visual field representation (for example, above 3.5° eccentricity: V1, $p = 4 \times 10^{-4}$; V2, $p = 0.12$; V3, $p = 0.03$). The mean pRF size at the same eccentricity grouped across all

subjects is similarly significantly correlated with eccentricity in all visual field maps (Supplementary Fig. 3A). Upper quadrant CMFs also decrease more strongly with eccentricity than lower quadrant CMFs in V1, V2 and V3 (Fig. 2D). The mean CMF at the same eccentricity grouped across all subjects is similarly significantly correlated with eccentricity in all visual field maps (Supplementary Fig. 4B). Therefore, relative to the lower quadrant, the representation of the upper quadrant becomes coarser with eccentricity.

If we again express pRF size differences as the ratio of pRF size, and CMF differences as a ratio of inverse CMF, we again find that the lower quadrant of V1 has smaller pRF sizes than the upper quadrant (V1:

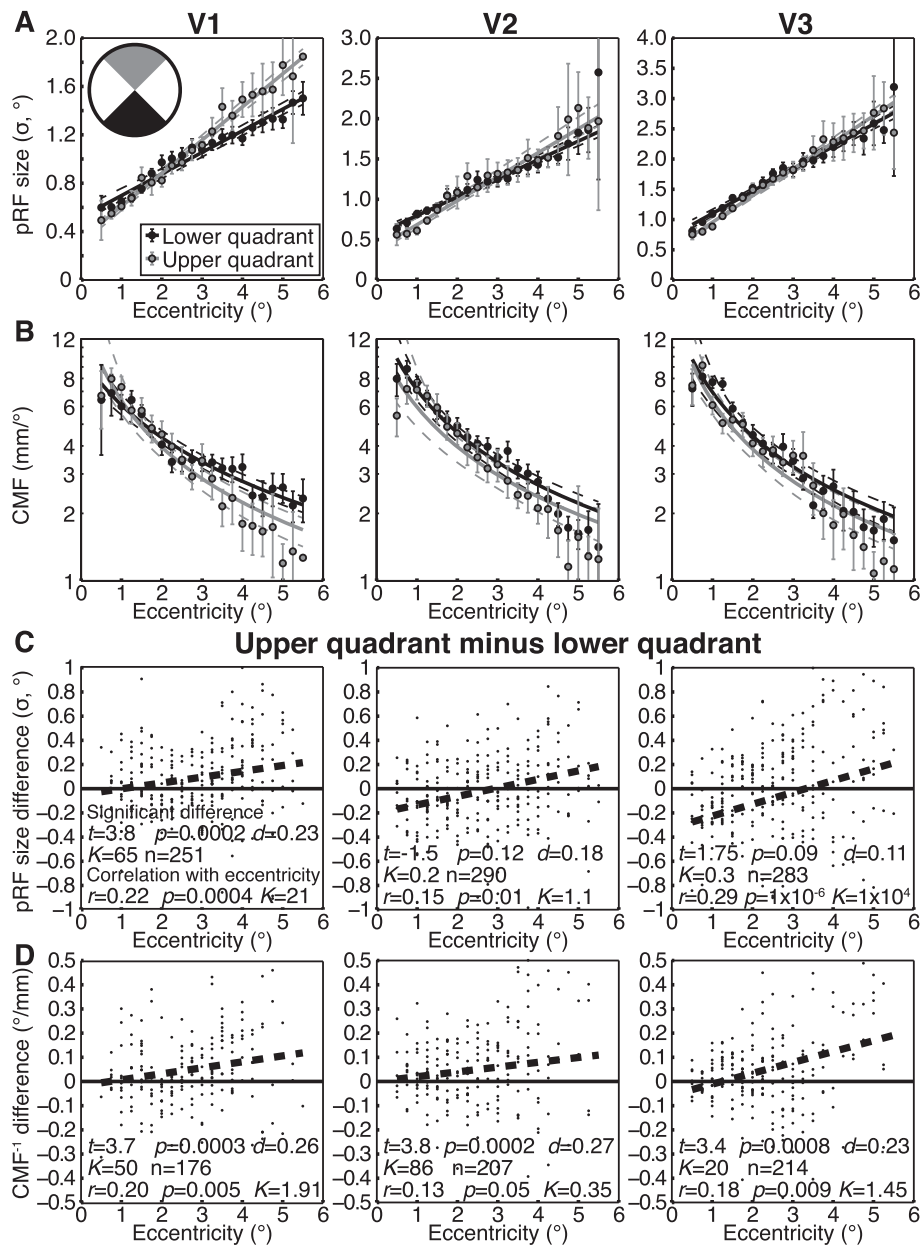


Fig. 2. Comparisons of pRF size and CMF between groups of recording sites in quadrants centered around the upper and lower vertical visual field meridians, paired for eccentricity and subject identity. (A) In data grouped across all subjects, pRF sizes increase with eccentricity. (B) CMF decreases with eccentricity and CMFs are larger in the lower quadrant. (C) When differences between paired bins from individual subjects are grouped together across all eccentricities pRF sizes are larger in the upper than the lower quadrant in V1, but not significantly different in V2 or V3. However, in the central visual field representation, pRF sizes are typically smaller in the upper than the lower quadrant. The increase of pRF size with eccentricity is greater in the upper quadrant, so pRF sizes are typically larger in the upper quadrant at higher eccentricities. (D) CMFs are larger in lower than the upper quadrant in V1, V2, and V3. This difference increases with eccentricity.

$t = 3.1, p = 0.0016, n = 265$), but the lower quadrant of V2 has larger pRF sizes than the upper quadrant (V2: $t = 4.6, p = 7 \times 10^{-6}, n = 277$) and V3 shows no significant difference (V3: $t = 1.9, p = 0.051, n = 272$). In all visual field maps, converting pRF size differences to a ratio of pRF size introduces a correlation between pRF size difference and eccentricity (V1: $r = 0.16, p = 0.011, n = 265$. V2: $r = 0.19, p = 0.0017, n = 277$. V3: $r = 0.31, p = 1 \times 10^{-7}, n = 272$). As before conversion to a ratio of CMF, lower quadrants of V1, V2 and V3 have larger CMFs than the upper quadrants (V1: $t = 3.5, p = 0.0006, n = 201$. V2: $t = 3.8, p = 0.0002, n = 209$. V3: $t = 3.4, p = 0.0007, n = 223$), but CMF differences are no longer significantly correlated with eccentricity. Across all eccentricities, the CMF difference between upper and lower quadrants remains about 18.1% of V1's inverse CMF, 16.5% of V2's inverse CMF and 12.7% of V3's inverse CMF.

pRF sizes are smaller in the left than the right quadrants in V2 and V3

We find the least clear differences between right and left visual field quadrants (Fig. 3). The right quadrants of V2 and V3 have larger pRF sizes than the left quadrants (Fig. 3A and C). However, the effect sizes here are very small, there is no significant difference in V1, and the difference in V2 does not reach significance if differences at the same eccentricities are averaged across subjects before comparison (Supplementary Fig. 6A). Therefore, we are less confident of these differences than the other differences we report.

Here we find no significant differences in CMF between left and right quadrants (Fig. 3B and D, Supplementary Figs. 6 and 7). We find no effects of eccentricity on differences in pRF size or CMF between left and right quadrants (Fig. 3C and D). We also find no effects of eccentricity if

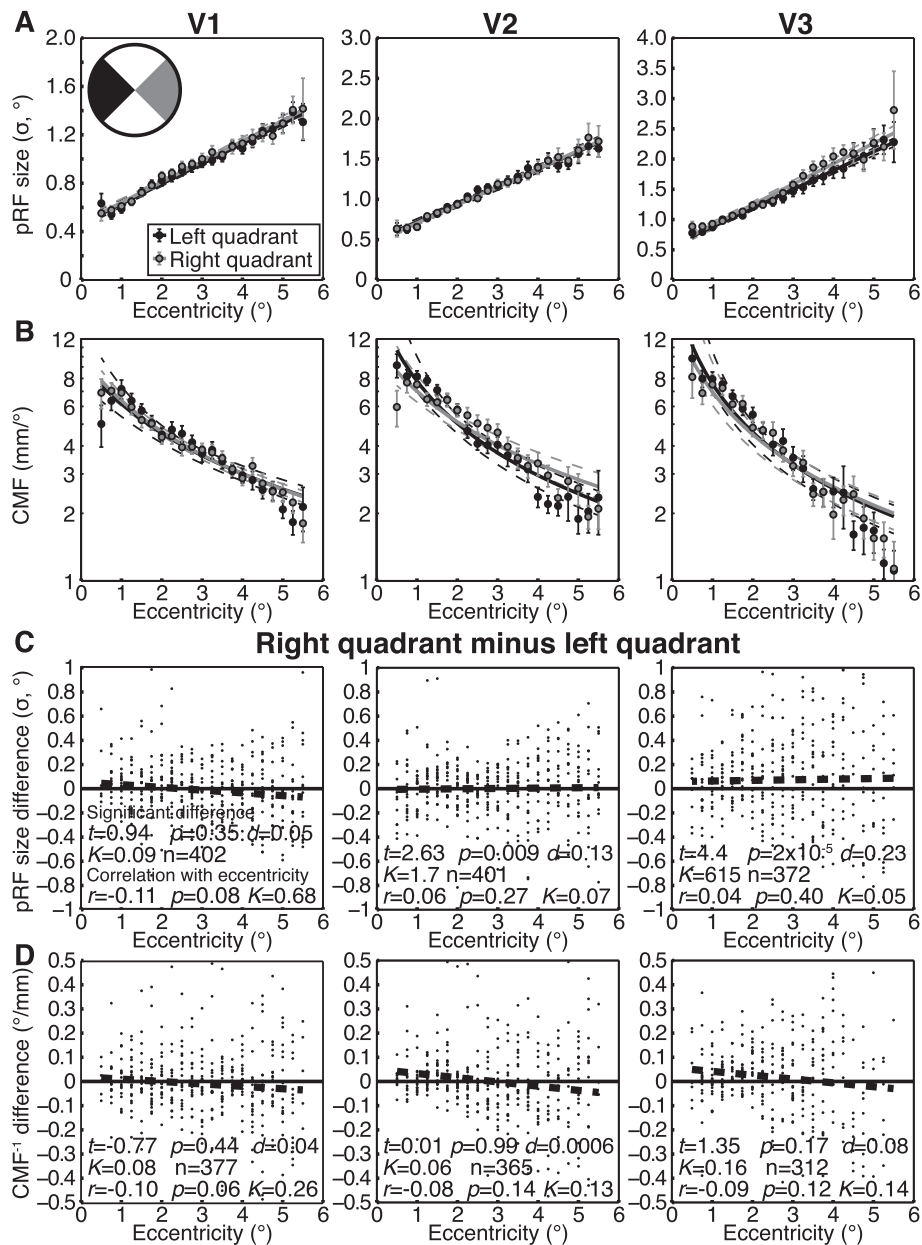


Fig. 3. Comparisons of pRF size and CMF between groups of recording sites in quadrants centered around the left and right horizontal visual field meridians, paired for eccentricity and subject identity. (A) In data grouped across all subjects, pRF sizes increase with eccentricity. (B) CMF decreases with eccentricity. (C) Differences between paired bins from individual subjects show that pRF sizes are significantly larger in right than the left quadrant in V2 and V3, but not significantly different in V1. (D) CMFs are not significantly different between left and right quadrants. There are no significant correlations with eccentricity.

grouping across subjects first (Supplementary Fig. 6). Data from individual subjects is shown in Supplementary Fig. 7.

If we again express pRF size differences as the ratio of pRF size, and CMF differences as a ratio of inverse CMF, we again find that the right quadrant of V3 has larger pRF sizes than the left quadrant ($t = 5.0$, $p = 1 \times 10^{-6}$, $n = 368$). No other differences or correlations reach significance.

Systematic and gradual pRF size and CMF change across polar angle

Differences between quadrants could be driven by differences at the horizontal and vertical meridians only, or could result from gradual changes in pRF size and CMF across the visual field map. Therefore, we finally determine how pRF size and CMF change with finer changes in polar angle. Because pRF size and CMF change considerably across eccentricity, we first regress out effects of eccentricity seen in the data

combined across all quadrants (see Methods). This reveals the progression of pRF sizes with polar angle shown in Fig. 4. This provides an overview of many effects seen in Figs. 1–3, and includes some finer-scale details. However, this overview disregards the changes we see across eccentricity. Rather than presenting statistical comparisons between the many polar angle bins, we show where differences between individual bins reach significance using the 95% confidence intervals given in Fig. 4.

pRF sizes gradually decrease approaching the horizontal meridian and increase approaching the vertical meridians in V1, V2 and V3 (Fig. 4A). This effect progresses gradually over much of the polar angle range, and is not limited to the horizontal and vertical meridians.

Progressions of CMF with polar angle are less clear than progressions of pRF size, as CMF data are noisier (Fig. 4B). However, these data generally continue to reflect the inverse relationship between pRF size and CMF. In contrast to pRF sizes, CMFs are typically larger near the horizontal meridian and smaller near the vertical meridians.

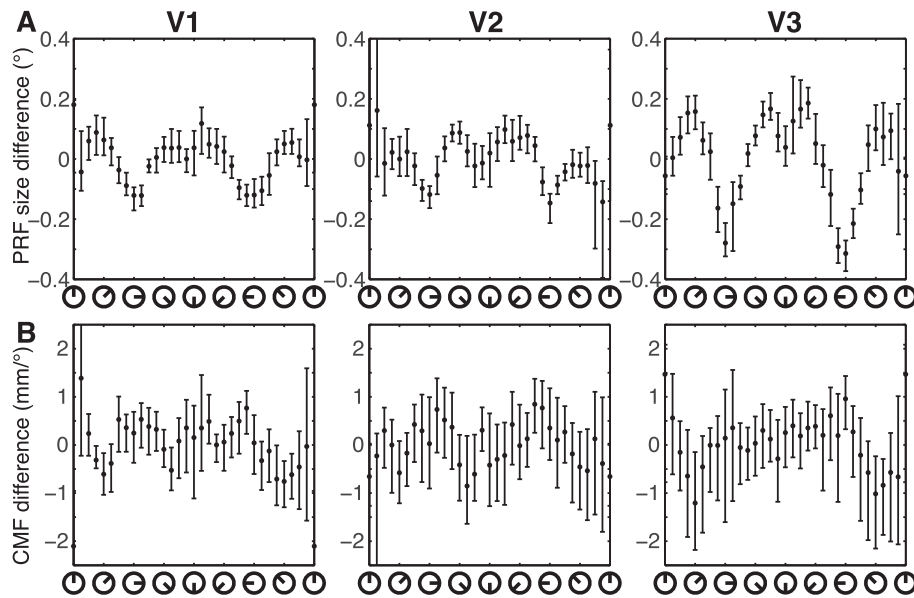


Fig. 4. Progression of pRF size and CMF with polar angle, after compensating for their changes with eccentricity. (A) pRF sizes gradually decrease approaching the horizontal meridians and increase approaching the vertical meridians. (B) CMFs typically increase approaching the horizontal meridians and decrease approaching the vertical meridians. However, these data are far noisier than pRF data, and become unreliable near the discontinuities in the visual field maps. Points show medians in each polar angle bin. Error bars are 95% confidence intervals of these medians, determined by bootstrapping data at the subject level.

Relationship of pRF size and CMF to cortical curvature

V1 has a strong relationship between cortical curvature and the polar angle of its visual field representation. V1's horizontal meridian representation lies in the fundus of the calcarine sulcus, which has a positive (concave) curvature. Progressing to the vertical meridian representation, V1 crosses the banks of the calcarine sulcus (relatively flat), then turns onto the cortex's medial surface through a negative (convex) curvature just before reaching the vertical meridian representation. It is therefore possible that differences in V1's cortical curvature rather than polar angle produce the changes in pRF size and CMF in V1. V2 and V3 do not have such clear relationships between cortical curvature and the polar angle representation.

We tested for relationships of cortical curvature to pRF size and CMF after first regressing out effects of eccentricity seen in the data combined across all quadrants (Fig. 5). This shows the expected negative correlation of pRF size to cortical curvature in V1 (Fig. 5A). Positive curvatures are found with smaller pRF sizes, likely because both are found in the horizontal quadrant representations. Negative curvatures are found with larger pRF sizes, likely because both are found in the vertical quadrant representations. In V2, we find the opposite: a weaker positive correlation of pRF size to cortical curvature. We find no relationship of pRF size to cortical curvature in V3. We found no significant correlation of CMF to cortical curvature in V1, V2 or V3 (Fig. 5B), perhaps because CMF data are noisier.

Therefore, pRF size is only correlated with cortical curvature when

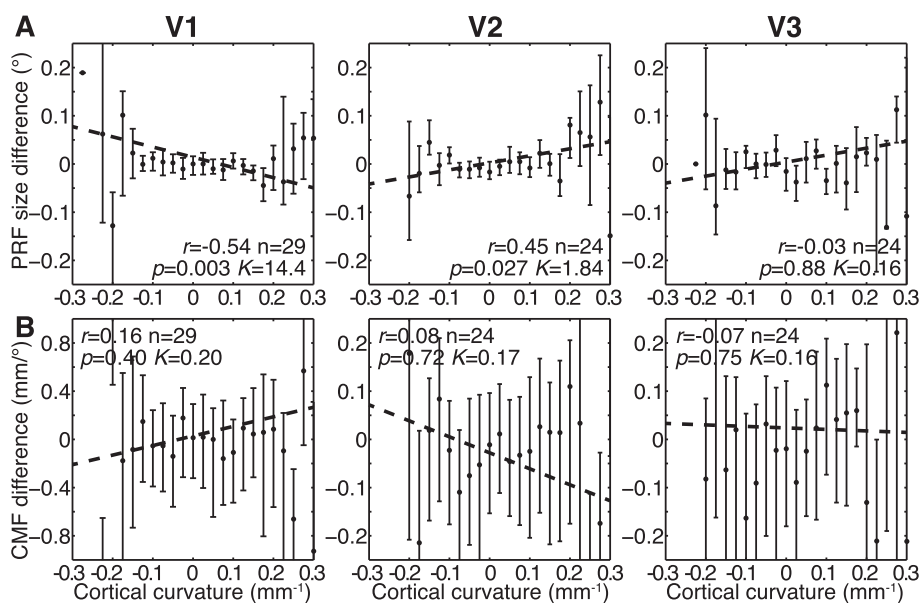


Fig. 5. Progression of pRF size and CMF with cortical curvature, after compensating for their changes with eccentricity. (A) In V1, pRF sizes decrease with increasing cortical curvature. The opposite relationship is seen in V2, and no relationship is seen in V3. (B) CMFs show no significant relationship to cortical curvature. However, these data are far noisier than pRF data. Points show medians in each polar angle bin. Error bars are 95% confidence intervals of these medians, determined by bootstrapping data at the subject level.

cortical curvature has a strong relationship to polar angle, suggesting that polar angle differences between quadrants underlie radial asymmetries in pRF size and CMF.

Discussion

Summary

We used computational neuroimaging approaches to ask how population receptive field (pRF) sizes and cortical magnification factors (CMFs) change across polar angle in early visual cortex (V1 to V3). We first compared groups of recording sites in different visual field quadrants at the same eccentricities and in the same subjects. We found smaller pRFs and larger CMFs in the horizontal than vertical quadrants in all three visual field maps, both suggesting a finer representation of visual space in the horizontal quadrants. Furthermore, pRF sizes increased and CMFs decreased more strongly with eccentricity in the vertical quadrants than the horizontal quadrants, so pRF size and CMF differences here were approximately proportional to average pRF size and CMF. CMFs were also larger in the lower than upper quadrant, and again differences increased with eccentricity, proportionally to CMF. However, pRF size differences between upper and lower quadrants changed direction with eccentricity in V2 and V3. pRF sizes were typically smaller in the upper than the lower quadrant up to about 2.5° eccentricity, but increased more with eccentricity, so were typically larger in the upper quadrant at higher eccentricities. pRFs were very slightly smaller in the left than right quadrant in V2 and V3, but there was no difference in V1 and no difference between CMFs, so differences between left and right quadrants were less clear and consistent than other findings. pRF size changed gradually with polar angle, decreasing and increasing smoothly when approaching the horizontal and vertical meridians, respectively. CMF changed less clearly, but conversely increased towards the horizontal meridian. Neither pRF size nor CMF differences consistently follow patterns of cortical curvature. Overall, there were small but highly significant differences in pRF size and CMF with polar angle: the early human visual cortex does not have a radially symmetric representation of the visual field.

Relationship to neurophysiological studies

It is difficult to densely and evenly sample RF properties across a single animal's visual field map using neurophysiological approaches. A few studies have investigated CMF (but not RF/pRF size) differences between V1's horizontal and vertical meridians. These have used various methods and species, sometimes producing conflicting results.

Van Essen, Newsome and Maunsell (1984) determined hundreds of RF locations along multiple electrode penetrations in individual *Macaca fascicularis*. They found larger CMFs along the horizontal than vertical meridian, and a slightly larger CMF in the lower than upper vertical meridian, like our results. This larger CMF at the lower vertical meridian is also corroborated by human fMRI results showing larger cortical activations for stimuli presented at the lower than the upper vertical meridian (Liu et al., 2006). Van Essen and colleagues also note considerable variability between individual animals in these trends, and in V1's shape. They also showed highly anisotropic rates of visual field progression at the vertical meridian, so CMF depended whether progressing along polar angle or eccentricity directions. Human fMRI shows similar anisotropies (Larsson and Heeger, 2006). Our CMF measurements compared mean cortical and visual field distances between recording sites and their neighbors, regardless of direction.

Tootell et al. (1988) presented flickering grids to various macaque species while staining V1 for glucose metabolism. They primarily examined the progression of linear CMF along the eccentricity direction, and conversely describe larger CMFs along the vertical than horizontal meridian. They also found large anisotropies at the vertical meridian, so found no consistent differences in areal CMF, which (like our approach)

considers both polar angle and eccentricity directions.

Finally, Adams and Horton (2003) mapped cortical projections of retinal blood vessels to determine the correspondence between retinal and cortical locations in two squirrel monkeys (*Saimiri sciureus*). Retinal angles differ slightly from visual angles (Perry and Cowey, 1985). Blood vessels are too small for this procedure in the central 4°, so they used Cowey's (1964) squirrel monkey retinotopic map here. They found a longer vertical than horizontal meridian, with more than twice the difference reported elsewhere (Daniel and Whitteridge, 1961; Tootell et al., 1988). Unlike Tootell et al. (1988) and Van Essen, Newsome and Maunsell (1984), they found a longer upper than lower vertical meridian. In the eccentricity progression, CMF gradually decreased approaching the horizontal meridian, but areal CMF (including directional anisotropies) changed little with polar angle.

In summary, these studies examined small numbers of animals of different primate species, reported differences between individuals, and suggested differences between species. Therefore, we examined a larger number of individual humans.

Methodological and physiological considerations

fMRI can straightforwardly measure pRF size and CMF throughout multiple visual field maps because it simultaneously records responses of densely and evenly distributed sites. It can also test large numbers of individuals as clear pRF maps require less than 1 hour of scanning per individual.

pRF properties reflect both single neuron RFs and the recording site's RF distribution. Do our pRF size differences reflect single neuron RF size differences? RF scatter (the distribution of RFs positions at a single recording site) is proportional to RF size (Albright and Desimone, 1987; Dow et al., 1981; Fiorani et al., 1989; Gattass and Gross, 1981; Hubel and Wiesel, 1974), so RF scatter differences should indirectly reflect RF size differences.

Could pRF size and CMF differences arise from visual field map discontinuities alone? Two results argue against this. First, pRF size and CMF vary gradually with polar angle, rather than changing at the meridians only. Second, V1's horizontal meridian has no discontinuity, but (just like V2's and V3's) has a pRF size minimum and CMF maximum.

Specifically, could partial voluming of signals across visual field map borders underlie the differences we see? Near the border between V1 and V2, there could be partial voluming of V1 and V2 signals, increasing V1 pRF sizes and decreasing V2 pRF sizes near their vertical meridians. However, while V1 pRF sizes do indeed increase in the vertical quadrants (near the border with V2), V2 pRF sizes also increase (rather than decrease) here. Similarly, partial voluming of V2 and V3 signals would increase V2 pRF sizes and decrease V3 pRF sizes near their horizontal meridians. However, while V3 pRF sizes do indeed decrease in the horizontal quadrants, V2 pRF sizes also decrease, again opposite to the predictions of a partial voluming account. Partial voluming should also decrease the rate of visual field position change at all visual field map reversal borders, increasing CMF. However, CMF increases at some borders and decreases at others. CMF also increases towards V1's horizontal meridian, where there is no visual field map reversal, consistent with its progression across V2 and V3. Overall, pRF sizes and CMFs progress similarly with polar angle in different visual field maps, regardless of which visual field maps they border, and the pattern of these progressions is not consistent with that predicted by partial voluming.

However, there are small irregularities at the visual field map discontinuities. pRF sizes decrease and their confidence intervals increase at the vertical meridians. CMF confidence intervals increase at all discontinuities: the underlying pRF position comparisons exclude recording sites in neighboring visual field maps, so estimates here come from less data.

Could hemodynamic differences between the cortical areas representing different quadrants underlie the pRF size or CMF differences we

find? We tested for this possibility by fitting individual two-gamma HRFs to each recording site. No HRF parameter differed consistently between quadrants in different visual field maps, or followed the observed changes in pRF size or CMF. Furthermore, fitting pRF models using these recording site-specific HRFs yielded very similar pRF size and CMF differences between quadrants.

Could different extents of horizontal and vertical microsaccades (Engbert and Kliegl, 2003) underlie the differences between horizontal and vertical quadrants? Several details of our results make this interpretation unlikely. First, any eye movement transforms the entire visual field, not only the part to which the gaze moves (Klein et al., 2014; Levin et al., 2010). So eye movements anisotropies should affect pRF shape globally, not pRF size in a particular quadrant. Second, local effects would require increased eye movements when a particular part of the visual field is mapped, and increased eye movements with eccentricity. But, using highly accurate eye position recording outside of the scanner, we find that the spread of gaze positions is unaffected by the mapping stimulus's presence, position, or direction of progression. Third, improbably large eye movement differences between quadrants would be needed for the pRF size differences we see. Eye movements increase pRF size following a Gaussian convolution of the pRF and the spread of gaze positions. Because this is a Pythagorean addition, the gaze position spread would need to be 42% of the quadrants' average pRF size to produce the observed ~10% change in pRF size between horizontal and vertical quadrants. Assuming zero spread of gaze positions during horizontal quadrant mapping, gaze eccentricity must be beyond 0.42° for 32% of the time during vertical quadrant mapping to produce the difference observed in V1. This is far beyond the extent of microsaccades and easily detectable by eye tracking. Even larger spreads would be needed to produce the differences observed in V2 and V3, where the underlying pRFs are larger. No single pattern of eye movements could produce the differences observed in all visual field maps. Finally, microsaccade anisotropies would not systematically change the cortical surface area representing a quadrant, so would not affect CMF. The CMF differences we see are also consistent with V1 single neuron recordings from macaques (Van Essen et al., 1984). So, patterns of eye movements are unlikely to underlie the differences we find.

Do increasing differences in pRF size and inverse CMF with eccentricity result from changes in pRF size, CMFs or eccentricity itself? pRF size and inverse CMF are approximately proportional to eccentricity, so we cannot distinguish between progressions with pRF size or eccentricity. However, the differences that are largest and most repeatable between visual field maps (pRF size and CMF difference between horizontal and vertical quadrants, CMF difference between upper and lower quadrants) cease to change significantly across eccentricity when expressed as a proportion of baseline pRF size or CMF.

Relationship to visual perception

V1 sites representing visual field positions with higher visual acuity have larger CMFs (Duncan and Boynton, 2003). Individuals with higher visual acuity have smaller pRFs (Song et al., 2015). As pRF sizes and CMFs are closely linked within and between individuals (Harvey and Dumoulin, 2011), recording sites and individuals with smaller pRFs and larger CMFs seem to support finer visuo-spatial perception.

So, do differences in perceptual performance across polar angle follow pRF size and CMF differences? Visual perception exhibits polar angle asymmetries for various stimuli and tasks (Karim and Kojima, 2010), suggesting functionally heterogeneous visual field representations (Carrasco et al., 2002; Silva et al., 2008, 2010). Perceptual accuracy is higher at the horizontal meridian than the vertical meridian for Gabor detection in noise, Gabor orientation discrimination and Gabor position discrimination (Carrasco et al., 2001). Grating contrast detection thresholds are also lower at the horizontal meridian (Rijsdijk et al., 1980; Rovamo and Virsu, 1979) and subjects localize the gap in a Landolt square faster and more accurately at the horizontal than the vertical

meridian (Carrasco et al., 2002). These results are all in line with our finding that early visual spatial representations are finer for the horizontal than the vertical quadrants.

Similarly, Gabor orientation discrimination requires less contrast at the lower vertical meridian than the upper (Cameron et al., 2002); grating contrast detection thresholds are also lower at the lower meridian (Rijsdijk et al., 1980; Silva et al., 2008, 2010); contrast, hue and motion detection thresholds are lower in the lower hemifield (Levine and McAnany, 2005); and visually-guided pointing movements are both faster and more accurate in the lower than the upper visual field (Danckert and Goodale, 2001). These results are all consistent our finding that early visual spatial representations are finer in the lower than the upper quadrant.

Grating contrast detection thresholds are also lower at the left meridian than the right (Silva et al., 2008), and split brain patients show lower thresholds for vernier offset discrimination, line orientation discrimination and size discrimination in the left visual hemifield (Corballis et al., 2002). However, some results suggest that thresholds are lower in the left hemifield only for high spatial frequency stimuli, with lower thresholds in the right hemifield for low spatial frequency stimuli (Christman et al., 1991). So, although broadly in agreement with our finding of smaller left than right quadrant pRFs in V2 and V3, both perceptual and neurophysiological differences between the left and right quadrants are less consistent than other differences.

The perceptual performance measures described above have been replicated widely, and we see little value in further replications. However, it would be valuable to correlate individual differences in pRF/CMF effect sizes to individual differences in perceptual effects. We do not attempt this for several reasons. First, the pRF size and CMF differences we describe are small, at most 20% of the baseline pRF size or CMF. Using large numbers of subjects, the large individual differences in pRF size and V1 surface area (which vary by 200–300% between subjects) have recently been correlated to perceptual performance (Moutsiana et al., 2016; Schwarzkopf et al., 2011; Song et al., 2015), but no such correlations have been shown for smaller effect sizes like those we find. It may be possible to correlate individual differences in perceptual radial asymmetries to differences in pRF size or CMF radial asymmetries, but we believe even larger numbers of subjects would be needed, together with very good quality behavioral and fMRI data. Second, perceptual asymmetries across polar angle are typically studied at the group level, and are not found consistently in individual subject performance. Third, perceptual asymmetries are rarely examined within our 6.25° stimulus radius. They are typically studied at around 20° eccentricity, which may increase their size and detectability: our results suggest increasing neural effect sizes with eccentricity. However, perceptual asymmetries have been described at 4.5° (Cameron et al., 2002) and 3.2° eccentricity (Carrasco et al., 2001), so are certainly present within our eccentricity range. Given these limitations, we cannot conclusively demonstrate the differences we see in pRF size and CMF cause the perceptual asymmetries, despite similar patterns of effects.

We do not find differences in pRF size and CMF in all visual field maps. However, for several reasons, we do not propose that perceptual asymmetries depend only on visual field maps where we found significant differences. Nor do we propose that perceptual asymmetries result from pRF size differences where we found no significant CMF differences (or vice versa). First, more sensitive experiments may reveal significant differences in comparisons where we find none. Second, psychophysics experiments have used various stimuli and tasks, and the neural basis of task performance is not always clear. Third, these psychophysics experiments used stimuli at higher eccentricities than we tested, and cortical asymmetries change with eccentricity. Fourth, computational models suggest that neural populations with larger RFs can hold more accurate position information (Serenó and Lehky, 2011). Therefore, comparisons between performance and effects in specific areas may be more complex than they appear (Harvey and Dumoulin, 2016).

Finally, recent results suggest that differences between lower and

upper visual field extents may account for different extents of crowding in the lower and upper hemifields (Fortenbaugh et al., 2015). Could scaling of the visual field representation by visual field extent explain the pattern of results we see? The lower visual field extent is less than the upper visual field extent (Niederhauser and Mojon, 2002), which might account for the higher CMF (and accompanying lower pRF size) in the lower visual field, if the visual field representation were scaled by visual field extent. However, both vertical meridians have smaller extents than both horizontal meridians, which would predict a higher CMF (and lower pRF size) in the vertical than the horizontal quadrants, while we find the opposite. So anisotropies in visual field extent do not seem to underlie the asymmetries we find.

Conclusions

Human early visual field representations are not radially symmetrical in pRF size or visual field map organization. Opposite changes of RF/pRF size and CMF across polar angle follow similar inverse relationships across eccentricity (Hubel and Wiesel, 1974), and between individuals (Harvey and Dumoulin, 2011). Similar effects in V1, V2 and V3 extend links between the properties of nearby visual field maps. Perceptual performance shows radial asymmetries that may arise from this asymmetrical neural representation of visual space.

Acknowledgements:

This work was supported by the Netherlands Organization for Scientific Research (#452.08.008 to SD, #433.09.223 to SD and FW Cornelissen) and by the Portuguese Foundation for Science and Technology (#IF/01405/2014 to BH, #BPD/72029/2010 to MFS, #E-Rare4/0001/2012 to SF, #UID/4539/2013 to MCB).

Appendix A. Supplementary data

Supplementary data related to this article can be found at <https://doi.org/10.1016/j.neuroimage.2017.11.021>.

References

- Adams, D.L., Horton, J.C., 2003. A precise retinotopic map of primate striate cortex generated from the representation of angioscotomas. *J. Neurosci.* 23, 3771–3789.
- Albright, T.D., Desimone, R., 1987. Local precision of visuotopic organization in the middle temporal area (MT) of the macaque. *Exp. Brain Res.* 65, 582–592.
- Brainard, D.H., 1997. The psychophysics toolbox. *Spat. Vis.* 10, 433–436.
- Cameron, E.L., Tai, J.C., Carrasco, M., 2002. Covert attention affects the psychometric function of contrast sensitivity. *Vis. Res.* 42, 949–967.
- Carrasco, M., Evert, D.L., Chang, I., Katz, S.M., 1995. The eccentricity effect: target eccentricity affects performance on conjunction searches. *Percept. Psychophys.* 57, 1241–1261.
- Carrasco, M., Talgar, C.P., Cameron, E.L., 2001. Characterizing visual performance fields: effects of transient covert attention, spatial frequency, eccentricity, task and set size. *Spat. Vis.* 15, 61–75.
- Carrasco, M., Williams, P.E., Yeshurun, Y., 2002. Covert attention increases spatial resolution with or without masks: support for signal enhancement. *J. Vis.* 2, 467–479.
- Christman, S., Kitterle, F.L., Hellige, J., 1991. Hemispheric asymmetry in the processing of absolute versus relative spatial frequency. *Brain Cogn.* 16, 62–73.
- Corballis, P.M., Funnell, M.G., Gazzaniga, M.S., 2002. Hemispheric asymmetries for simple visual judgments in the split brain. *Neuropsychologia* 40, 401–410.
- Cowey, A., 1964. Projection of the retina on to striate and prestriate cortex in the squirrel monkey, *Saimiri sciureus*. *J. Neurophysiol.* 27, 366–393.
- Dahlem, M.A., Tusch, J., 2012. Predicted selective increase of cortical magnification due to cortical folding. *J. Math. Neurosci.* 2, 14.
- Danckert, J., Goodale, M.A., 2001. Superior performance for visually guided pointing in the lower visual field. *Exp. Brain Res.* 137, 303–308.
- Daniel, M., Whitteridge, D., 1961. The representation of the visual field on the cerebral cortex in monkeys. *J. Physiology* 159, 203–221.
- Dougherty, R.F., Koch, V.M., Brewer, A.A., Fischer, B., Modersitzki, J., Wandell, B.A., 2003. Visual field representations and locations of visual areas V1/2/3 in human visual cortex. *J. Vis.* 3, 586–598.
- Dow, B.M., Snyder, A.Z., Vautin, R.G., Bauer, R., 1981. Magnification factor and receptive field size in foveal striate cortex of the monkey. *Exp. Brain Res.* 44, 213–228.
- Dumoulin, S.O., Wandell, B.A., 2008. Population receptive field estimates in human visual cortex. *Neuroimage* 39, 647–660.
- Duncan, R.O., Boynton, G.M., 2003. Cortical magnification within human primary visual cortex correlates with acuity thresholds. *Neuron* 38, 659–671.
- Engbert, R., Kliegl, R., 2003. Microsaccades uncover the orientation of covert attention. *Vis. Res.* 43, 1035–1045.
- Engel, S.A., Rumelhart, D.E., Wandell, B.A., Lee, A.T., Glover, G.H., Chichilnisky, E.J., Shadlen, M.N., 1994. fMRI of human visual cortex. *Nature* 369, 525.
- Fiorani Jr., M., Gattass, R., Rosa, M.G., Sousa, A.P., 1989. Visual area MT in the Cebus monkey: location, visuotopic organization, and variability. *J. Comp. Neurol.* 287, 98–118.
- Fortenbaugh, F.C., Silver, M.A., Robertson, L.C., 2015. Individual differences in visual field shape modulate the effects of attention on the lower visual field advantage in crowding. *J. Vis.* 15.
- Friston, K.J., Fletcher, P., Josephs, O., Holmes, A., Rugg, M.D., Turner, R., 1998. Event-related fMRI: characterizing differential responses. *Neuroimage* 7, 30–40.
- Gattass, R., Gross, C.G., 1981. Visual topography of striate projection zone (MT) in posterior superior temporal sulcus of the macaque. *J. Neurophysiol.* 46, 621–638.
- Glover, G.H., 1999. Deconvolution of impulse response in event-related BOLD fMRI. *Neuroimage* 9, 416–429.
- Harvey, B.M., Dumoulin, S.O., 2011. The relationship between cortical magnification factor and population receptive field size in human visual cortex: constancies in cortical architecture. *J. Neurosci.* 31, 13604–13612.
- Harvey, B.M., Dumoulin, S.O., 2016. Visual motion transforms visual space representations similarly throughout the human visual hierarchy. *Neuroimage* 127, 173–185.
- Hubel, D.H., Wiesel, T.N., 1974. Uniformity of monkey striate cortex: a parallel relationship between field size, scatter, and magnification factor. *J. Comp. Neurol.* 158, 295–305.
- Karim, A.K., Kojima, H., 2010. The what and why of perceptual asymmetries in the visual domain. *Adv. Cogn. Psychol.* 6, 103–115.
- Klein, B.P., Harvey, B.M., Dumoulin, S.O., 2014. Attraction of position preference by spatial attention throughout human visual cortex. *Neuron* 84, 227–237.
- Larsson, J., Heeger, D.J., 2006. Two retinotopic visual areas in human lateral occipital cortex. *J. Neurosci.* 26, 13128–13142.
- Levin, N., Dumoulin, S.O., Winawer, J., Dougherty, R.F., Wandell, B.A., 2010. Cortical maps and white matter tracts following long period of visual deprivation and retinal image restoration. *Neuron* 65, 21–31.
- Levine, M.W., McAnany, J.J., 2005. The relative capabilities of the upper and lower visual hemifields. *Vis. Res.* 45, 2820–2830.
- Liu, T., Heeger, D.J., Carrasco, M., 2006. Neural correlates of the visual vertical meridian asymmetry. *J. Vis.* 6, 1294–1306.
- Moutsiana, C., de Haas, B., Papageorgiou, A., van Dijk, J.A., Balraj, A., Greenwood, J.A., Schwarzkopf, D.S., 2016. Cortical idiosyncrasies predict the perception of object size. *Nat. Commun.* 7, 12110.
- Nestares, O., Heeger, D.J., 2000. Robust multiresolution alignment of MRI brain volumes. *Magn. Reson. Med.* 43, 705–715.
- Niederhauser, S., Mojon, D.S., 2002. Normal isopter position in the peripheral visual field in goldmann kinetic perimetry. *Ophthalmologica* 216, 406–408.
- Oldfield, R.C., 1971. The assessment and analysis of handedness: the Edinburgh inventory. *Neuropsychologia* 9, 97–113.
- Olman, C.A., Inati, S., Heeger, D.J., 2007. The effect of large veins on spatial localization with GE BOLD at 3 T: Displacement, not blurring. *Neuroimage* 34, 1126–1135.
- Pelli, D.G., 1997. The VideoToolbox software for visual psychophysics: transforming numbers into movies. *Spat. Vis.* 10, 437–442.
- Perry, V.H., Cowey, A., 1985. The ganglion cell and cone distributions in the monkey's retina: implications for central magnification factors. *Vis. Res.* 25, 1795–1810.
- Rijsdijk, J.P., Kroon, J.N., van der Wildt, G.J., 1980. Contrast sensitivity as a function of position on the retina. *Vis. Res.* 20, 235–241.
- Rovamo, J., Virsu, V., 1979. An estimation and application of the human cortical magnification factor. *Exp. Brain Res.* 37, 495–510.
- Schira, M.M., Tyler, C.W., Spehar, B., Breakspear, M., 2010. Modeling magnification and anisotropy in the primate foveal confluence. *PLoS Comput. Biol.* 6, e1000651.
- Schwarzkopf, D.S., Song, C., Rees, G., 2011. The surface area of human V1 predicts the subjective experience of object size. *Nat. Neurosci.* 14, 28–30.
- Sereno, A.B., Lehky, S.R., 2011. Population coding of visual space: comparison of spatial representations in dorsal and ventral pathways. *Front. Comput. Neurosci.* 4, 159.
- Sereno, M.I., Dale, A.M., Reppas, J.B., Kwong, K.K., Belliveau, J.W., Brady, T.J., Rosen, B.R., Tootell, R.B., 1995. Borders of multiple visual areas in humans revealed by functional magnetic resonance imaging. *Science* 268, 889–893.
- Silva, M.F., Maia-Lopes, S., Mateus, C., Guerreiro, M., Sampaio, J., Faria, P., Castelo-Branco, M., 2008. Retinal and cortical patterns of spatial anisotropy in contrast sensitivity tasks. *Vis. Res.* 48, 127–135.
- Silva, M.F., Mateus, C., Reis, A., Nunes, S., Fonseca, P., Castelo-Branco, M., 2010. Asymmetry of visual sensory mechanisms: electrophysiological, structural, and psychophysical evidences. *J. Vis.* 10, 26.
- Smith, A.T., Singh, K.D., Williams, A.L., Greenlee, M.W., 2001. Estimating receptive field size from fMRI data in human striate and extrastriate visual cortex. *Cereb. Cortex* 11, 1182–1190.
- Smith, S.M., Jenkinson, M., Woolrich, M.W., Beckmann, C.F., Behrens, T.E., Johansen-Berg, H., Bannister, P.R., De Luca, M., Drobnjak, I., Flitney, D.E., Niazy, R.K., Saunders, J., Vickers, J., Zhang, Y., De Stefano, N., Brady, J.M., Matthews, P.M., 2004. Advances in functional and structural MR image analysis and implementation as FSL. *Neuroimage* 23 (Suppl 1), S208–S219.
- Song, C., Schwarzkopf, D.S., Kanai, R., Rees, G., 2015. Neural population tuning links visual cortical anatomy to human visual perception. *Neuron* 85, 641–656.
- Strasburger, H., Rentschler, I., Jüttner, M., 2011. Peripheral vision and pattern recognition: a review. *J. Vis.* 11, 13.

- Teo, P.C., Sapiro, G., Wandell, B.A., 1997. Creating connected representations of cortical gray matter for functional MRI visualization. *IEEE Trans. Med. Imaging* 16, 852–863.
- Tootell, R.B., Switkes, E., Silverman, M.S., Hamilton, S.L., 1988. Functional anatomy of macaque striate cortex. II. Retinotopic organization. *J. Neurosci.* 8, 1531–1568.
- Van Essen, D.C., Newsome, W.T., Maunsell, J.H., 1984. The visual field representation in striate cortex of the macaque monkey: asymmetries, anisotropies, and individual variability. *Vis. Res.* 24, 429–448.
- Wandell, B.A., Chial, S., Backus, B.T., 2000. Visualization and measurement of the cortical surface. *J. Cogn. Neurosci.* 12, 739–752.
- Wandell, B.A., Dumoulin, S.O., Brewer, A.A., 2007. Visual field maps in human cortex. *Neuron* 56, 366–383.
- Winawer, J., Horiguchi, H., Sayres, R.A., Amano, K., Wandell, B.A., 2010. Mapping hV4 and ventral occipital cortex: the venous eclipse. *J. Vis.* 10.
- Worsley, K.J., Liao, C.H., Aston, J., Petre, V., Duncan, G.H., Morales, F., Evans, A.C., 2002. A general statistical analysis for fMRI data. *Neuroimage* 15, 1–15.